Transport in Porous Media **11:** 201–218, 1993.

Viscous Coupling in Two-Phase Flow in Porous Media and Its Effect on Relative Permeabilities

R. EHRLICH
Chevron Oil Field Research, PO Box 446, La Habra, CA 90633, U.S.A.

(Received: 4 June 1991; revised: 9 April 1992)

Abstract. An idealized model of a porous rock consisting of a bundle of capillary tubes whose cross-sections are regular polygons is used to assess the importance of viscous coupling or lubrication during simultaneous oil-water flow. Fluids are nonuniformly distributed over tubes of different characteristic dimension because of the requirements of capillary equilibrium and the effect of interfacial viscosity at oil-water interfaces is considered. With these assumptions, we find that the importance of viscous coupling depends on the rheology of the oil-water interface. Where the interfacial shear viscosity is zero, viscous coupling leading to a dependence of oil relative permeability on oil-water viscosity ratio for viscosity ratios greater than one is important for a range of pore cross-section shapes and pore size distributions. For nonzero interfacial shear viscosity, viscous coupling is reduced. Using values reported in the literature for crude oil-brine systems, we find no viscous coupling.

Key words. Porous medium model, two-phase flow, Darcy's law, relative permeabilities.

Nomenclature

Lower Case

a, b, c	Undertermined parameter sets in velocity distribution function
k	Permeability
n	Unit normal vector to o-w interface
r	Coordinate in cylindrical system
s	Number of sides of polygon tube cross section
v	Fluid velocity
z	Coordinate in cylindrical system

Upper Case

F, F_o, F_w	Coefficients in tube flow equation
Gp	Pressure Gradient
H	Interface mean curvature
J, J_1, J_2, J_3	Integrals defined by (A3) and (A11)–(A13)
M	Number of tube sizes
N	Defines number of undetermined parameter in velocity distribution
N_{ca}	Capillary number
N_ε	Dimensionless interfacial shear viscosity
P	Pressure
Q	Volume flow rate
R	Characteristic tube dimension (Figure A1)
S_o, S_w	Oil and water saturations
S_t, S_i	Tube wall and oil-water interface area
$V(m)$	Pore volume of tubes of dimension $R(m)$ in bundle

Greek Letters

ε	Interfacial shear viscosity
μ	Viscosity
σ	Interfacial tension
Θ	Coordinate in cylindrical system
Φ	Coordinate in second cylindrical system
τ	Stress tensor

Subscripts

o	Oil phase quantity
w	Water phase quantity
r	r-component of vector
Θ	Θ-component of vector

1. Introduction

The Darcy description of flow in porous media, although originally obtained empirically from observations of one-dimensional flow, has been shown to be theoretically correct within the assumptions of local volume averaging and Stokes flow and has been generalized to multi-dimensional flow in anisotropic materials (Slattery, 1972; Whitaker, 1986a). The extension of Darcy's law to two-phase flow with relative permeabilities for each phase dependent on saturation and pore structure but not on fluid viscosities, densities, or flow rates is an empirical extension of the single phase Darcy description based on the idea that each fluid flows in its own set of pore channels. Bear (1972) describes the experimental evidence supporting this model and the theoretical arguments for and against it and concludes that it is a 'good approximation for all practical purposes'. It remains the accepted approach for describing two-phase flow in petroleum reservoir engineering calculations (Peaceman, 1977; Aziz and Settari, 1979). Occasionally, however, data are reported which appear to contradict this model.

A number of authors have questioned the validity of the two-phase Darcy equation, specifically whether viscous coupling or lubrication of a nonwetting phase by a wetting film can be important. Some of the arguments are compelling. An important implication of this issue is that it causes us to question current practice for obtaining relative permeability data in the laboratory and using it in petroleum reservoir calculations. Among many assumptions inherent to the existing two-phase Darcy formulation is that laboratory relative permeability curves obtained by co-current flow of a fluid pair, water and oil for example, are valid for other fluid pairs with the same relative wetting even though properties such as viscosity ratio may be different. This paper examines the arguments made for questioning the validity of the conventional two-phase Darcy flow model. Previously reported laboratory measurements and pore model calculations are examined and critiqued. Some new calculations are presented to further investigate the idea of viscous coupling and to suggest where the conventional Darcy model may and may not apply. Finally, recommendations are made for some definitive experiments.

2. Previous Work

Early models of two-phase flow, such as that of Yuster (1951), used simple geometries such as co-axial flow in a single circular cylinder or segregated flow between parallel plates to infer a viscosity ratio dependence of relative permeability. Criticisms of such models are that (1) porous media are not single pores but networks of pores of different sizes in which fluids are nonuniformly distributed as a result of the requirements of capillary equilibrium, (2) such simple geometries do not exist in natural rocks even for single pores, and (3) even in these idealized models, the stable interface configurations may not be as assumed.

Models of two-phase flow in pore networks, most recently Lin and Slattery (1972) and Heiba *et al.*, (1983), have excluded the possibility of simultaneous flow in a single pore, and therefore would not predict viscous coupling.

Singhal and Somerton (1970) considered two-phase flow in an equilateral triangular channel. This type of model has the advantage of beginning to introduce pore cross-section irregularity and allows formation of stable arc menisci at the triangle apexes. Such menisci have structural and hydrodynamic similarities to pendular wetting films at grain boundaries in porous rocks. Their analysis shows an important viscosity ratio effect on relative permeability ratios calculated assuming co-current flow of wetting and nonwetting fluids.

Kalaydjian (1990) carried out a series of two-phase flow experiments in square capillary tubes. Based on this work, he proposed a new form of the two-phase Darcy equation which contains coupling terms as well as conventional relative permeabilities and suggests that it gives a more complete and rigorous description of two phase flow. Rose (1990) presented calculations based on the earlier Yuster work which supports this model.

Whitaker (1986b) analyzed two-phase flow in a general porous medium by local volume averaging. His result for conditions approximating a steady-state relative permeability determination supports the above arguments, giving a form of the two-phase Darcy equation which contains nontraditional terms representing the viscous drag of one fluid on the other.

Because of the complexities associated with flow experiments in naturally occurring porous media, literature data can be confusing and can usually be found to support any position. For example, Leverett (1939) showed oil-water relative permeabilities in sand packs to be independent of viscosity ratio for μ_o/μ_w ranging from 0.057 to 90. Another study often cited is that of Odeh (1959). In this, relative permeability to oil in a series of water-oil relative permeability measurements was found to increase with oil-water viscosity ratio, with values of k_{ro} as high as 240% reported. Odeh attributes this result to a lubrication effect.

3. Model Formulation and Calculations

In this section, we present two-phase oil-water flow calculations using an idealized model which nevertheless captures more of the attributes of real porous rocks pertinent to characterization of viscous coupling than models previously reported. Specifically, we consider that pore spaces have noncircular cross sections, range over an order of magnitude or more in size, and are highly interconnected. Local volume averaging concepts are then used to calculate relative permeabilities.
The following are the assumed idealizations.

(1) A unit volume can be defined which is large compared with the largest pore dimensions and contains a representative pore size distribution but is smaller than the macroscopic dimensions of the porous rock. Averaged quantities such

as saturations, space velocities, and pressures in each phase are constant within that volume.

(2) Individual pores are tubes whose cross-sections are regular polygons (equilateral triangle, square, etc.) as described in the Appendix.

(3) The capillary number, $N_{ca} = \mu v/\sigma_{ow}$, for flow in either phase is low. Gravity effects are negligible.

(4) The pores are water-wet (i.e. interfaces intersect the tube wall with 0° contact angle measured in the water phase).

(5) Velocity is continuous across oil-water interfaces.

(6) Two types of tangential stress boundary conditions at oil-water interfaces are considered.

   (a) Tangential stress is continuous. This is assumed to be the case for 'pure' fluids that are free of surface-active materials.

   (b) Discontinuity in tangential stress is defined by the Boussinesq Newtonian surface fluid model (Scriven, 1960; Aris, 1962). This attempts to consider accumulation of surface active materials that naturally occur in petroleum reservoir fluids. As noted in the Appendix, this discontinuity relates to the interfacial shear viscosity.

(7) The porous rock is assumed to consist of a 'bundle' of such tubes, all of which are of equal length and of geometrically similar cross-section, and are present according to a known pore size-pore volume distribution function. Interconnections between these pores exist and ensure that pressures in each phase are the same in every tube. However, they are assumed not to contribute to steady-state flow or to pore volume.

Note that this model is only intended to examine viscous coupling and does not rigorously consider aspects of pore interconnections that lead to flow path tortuosity and saturation hysteresis. Thus, calculated relative permeabilities will not have the appearance of real rock curves.

A porous rock containing this unit volume is assumed to have initially been water saturated and then to have been oil saturated by displacement of that water to some oil saturation close to 100%. At that point, a series of steady-state relative permeability measurements are made with water fractional flow increasing in steps from some low value to 1. Once a steady state is reached, it is assumed that the saturation distribution is fixed and there are no moving interfaces. It is further assumed that the unit volume is far from inlet or outlet boundaries and that the pressures in each phase differ by an oil-water capillary pressure.

Figure 1 shows a typical unit volume undergoing displacement. The capillary pressure defines an interface radius which must be common to all tubes in the bundle. It is assumed, as shown in Figure A1, that the largest stable interface radius corresponds to a circle internally tangent to the polygon cross-section. Increasing the tube water volume beyond that point results in instability and complete displacement of oil from the tube (Mason and Morrow, 1991). This

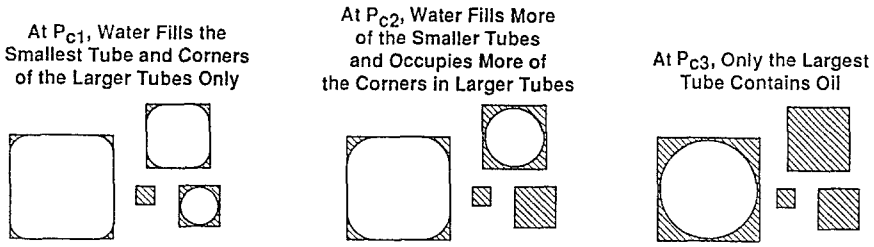

Fig. 1. Cross-section of unit cell composed of square capillary tubes at $P_{c1} > P_{c2} > P_{c3}$ (Note that oil-water interface curvature is the same in each tube at any Pc).

defines a minimum tube dimenson that will contain both phases. Smaller tubes will contain only water.

The volume of oil in each tube is calculated from the geometry relationships in Figure A1, choosing the interface configuration corresponding to the interface radius. Saturations and relative permeabilities are then calculated by summing the individual tube relationships over the unit volume. We assume that the tube bundle contains tubes of M different sizes and that all the tubes with characteristic radius $R(m)$ together have a volume $V(m)$, and that the fixed interface radius defines $S_w(m)$ in the individual tubes. Each $S_w(m)$ has a corresponding $F_w[S_w(m)]$ and $F_o[S_w(m)]$ so that

$$S_w = \frac{\sum_{m=1}^{m=M} S_w(m)V(m)}{\sum_{m=1}^{m=M} V(m)}, \tag{1}$$

$$K_{rw} = \frac{\sum_{m=1}^{m=M} F_w[S_w(m)]R^2(m)V(m)}{\sum_{m=1}^{m=M} F(m)R^2(m)V(m)}, \tag{2}$$

$$K_{ro} = \frac{\sum_{m=1}^{m=M} F_o[S_w(m)]R^2(m)V(m)}{\sum_{m=1}^{m=M} F(m)R^2(m)V(m)}. \tag{3}$$

Terms in Equations (1)–(3) are defined in the Appendix.

Using this procedure, oil-water relative permeabilities were calculated for different oil-water viscosity ratios, tube shapes, and pore size distributions. Calculations were also made for cases where tangential stress is and is not continuous (i.e. where interfacial shear viscosity is and is not negligible).

Figures 2 and 3 show oil and water relative permeabilities, respectively, as a function of viscosity ratio for a porous medium composed of a bundle of square cross-section tubes. The pore volume in this porous medium is uniformly distributed among tubes whose characteristic radii span one order of magnitude. That is,

$$V(m) = 1/M, \qquad R(m) = R_{\min} + (m-1)(R_{\max} - R_{\min})/(M-1),$$
$$\text{and} \quad R_{\max}/R_{\min} = 10$$

where $R_{\max}$ and $R_{\min}$ are dimensions of the largest and smallest tubes, respectively. In these calculations, values of M ranging from 10 to 100 were typically used.

Figure 4 shows k_{ro} vs. viscosity ratio for a bundle of 16-sided polygon cross-section tubes for the same assumed pore size distribution.

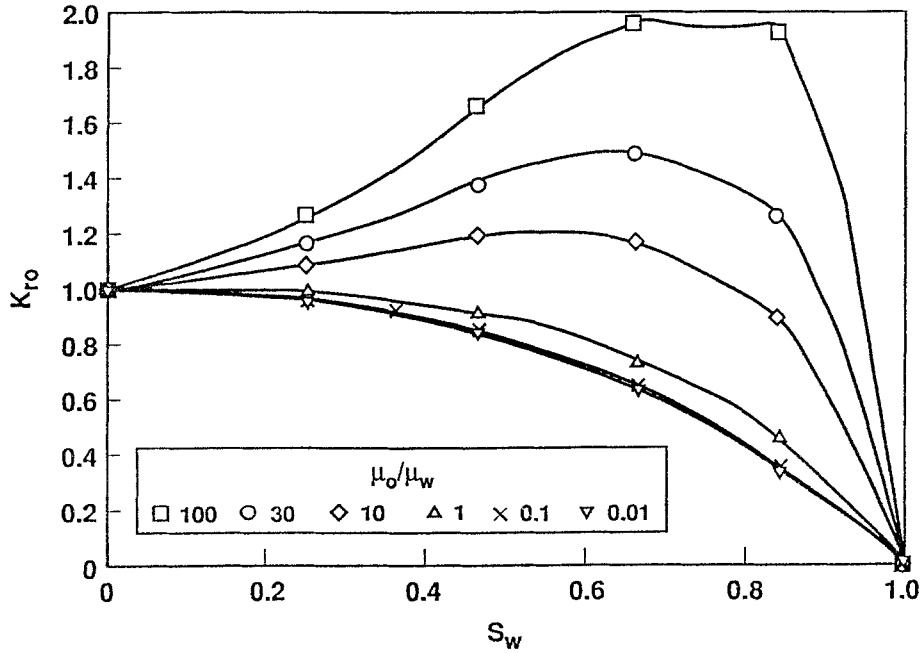

Fig. 2. K_{ro} vs oil:water viscosity ratio for a bundle of square tubes with $R_{max}/R_{min} = 10$.

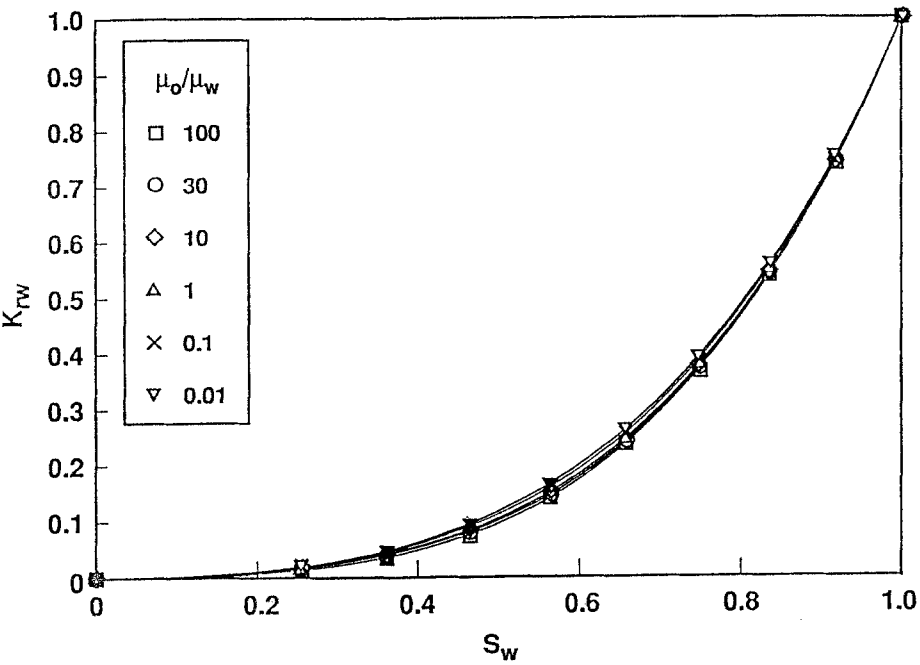

Fig. 3. K_{rw} vs oil:water viscosity ratio for a bundle of square tubes-with $R_{max}/R_{min} = 10$.

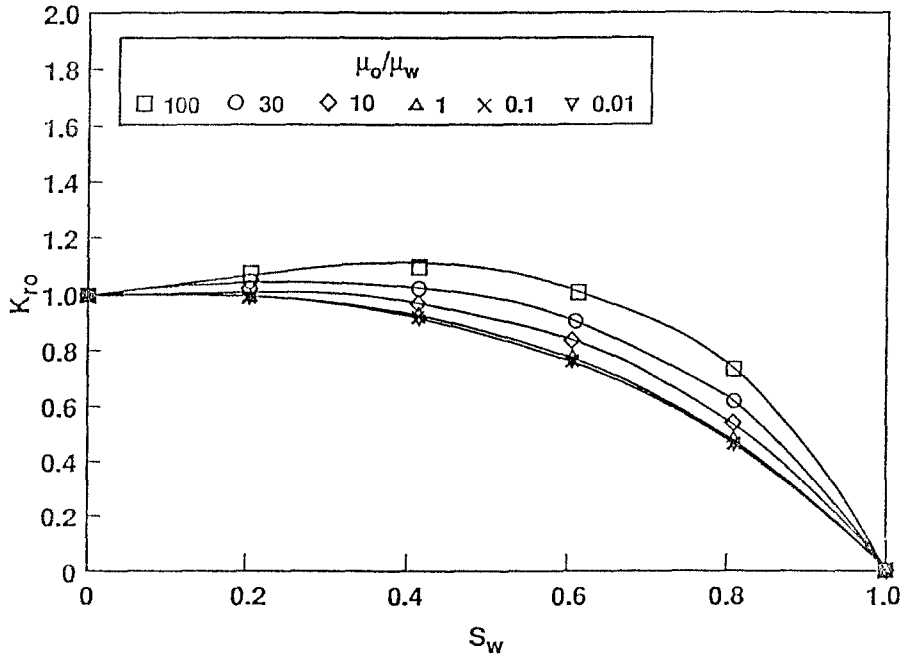

Fig. 4. K_{ro} vs oil:water viscosity ratio for a bundle of 16 side tubes-with $R_{max}/R_{min} = 10$.

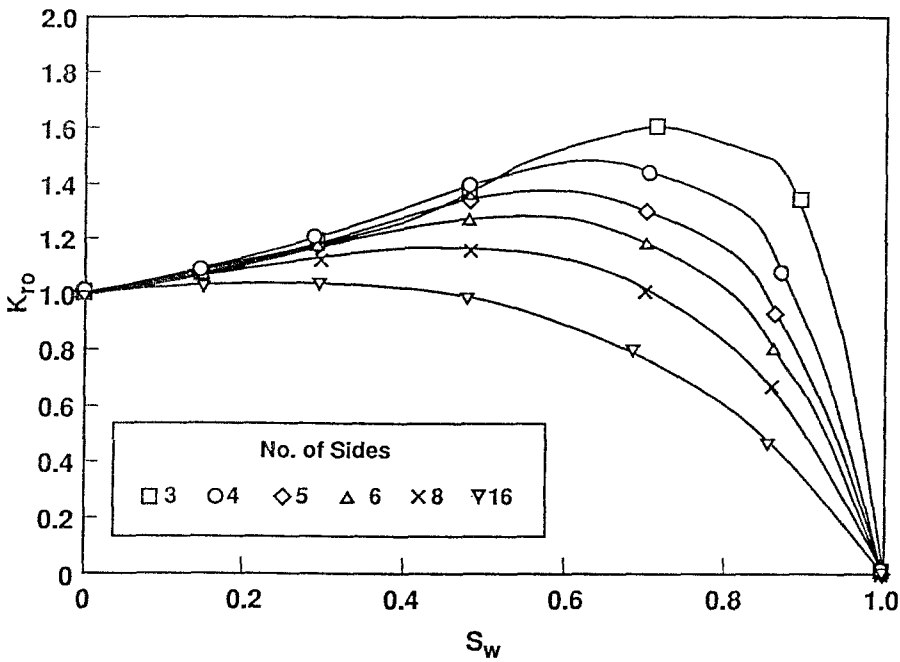

Fig. 5. K_{ro} vs number of sides of polygon for a bundle of polygonal cross-section tubes with $\mu_o/\mu_w = 30$ and $R_{max}/R_{min} = 10$.

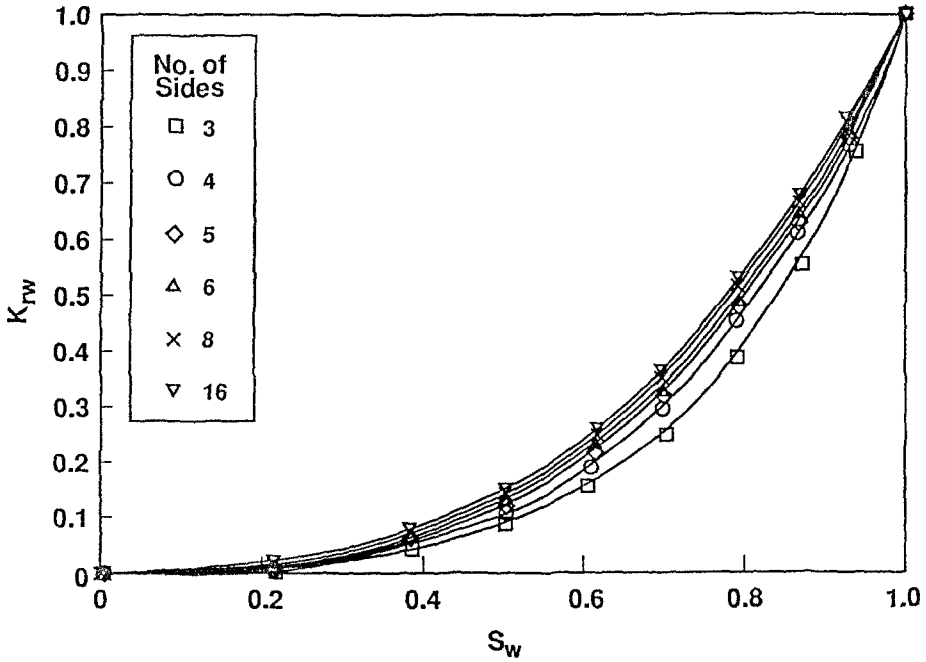

Fig. 6. K_{rw} vs number of sides of polygon for a bundle of polygonal cross-section tubes with $\mu_o/\mu_w = 30$ and $R_{max}/R_{min} = 10$.

Figures 5 and 6 show oil and water relative permeabilities as a function of the number of sides of the regular polygon tube cross-section. Oil-water viscosity ratio is fixed at 30 and the pore volume-pore size distribution is the same as above. Figures 7 and 8 show oil and water relative permeabilities as a function of the pore size distribution. Characteristic radii are assumed linearly distributed over several ranges with the ratio of R_{max} to R_{min} varying from 1.1 to 100. Again, identical fractional pore volumes are assigned to each pore radius. Oil-water viscosity ratio is fixed at 30 in this calculation and the individual tubes have square cross-sections.

Figures 9 and 10 show oil relative permeabilities for oil-water viscosity ratios of 10 and 100, respectively, as a function of a dimensionless interfacial shear viscosity

$$N_\varepsilon = \varepsilon/\mu_o R_{max} \tag{4}$$

where ε is the interfacial shear viscosity, R_{max} is the largest tube radius in the bundle, and μ_o is oil viscosity. Square cross-section tubes and a one order of magnitude pore size distribution are assumed.

4. Discussion

These results, first of all, clearly show lubrication of oil flow by water located in corners of the irregularly shaped tubes where interfacial shear viscosity is zero. For

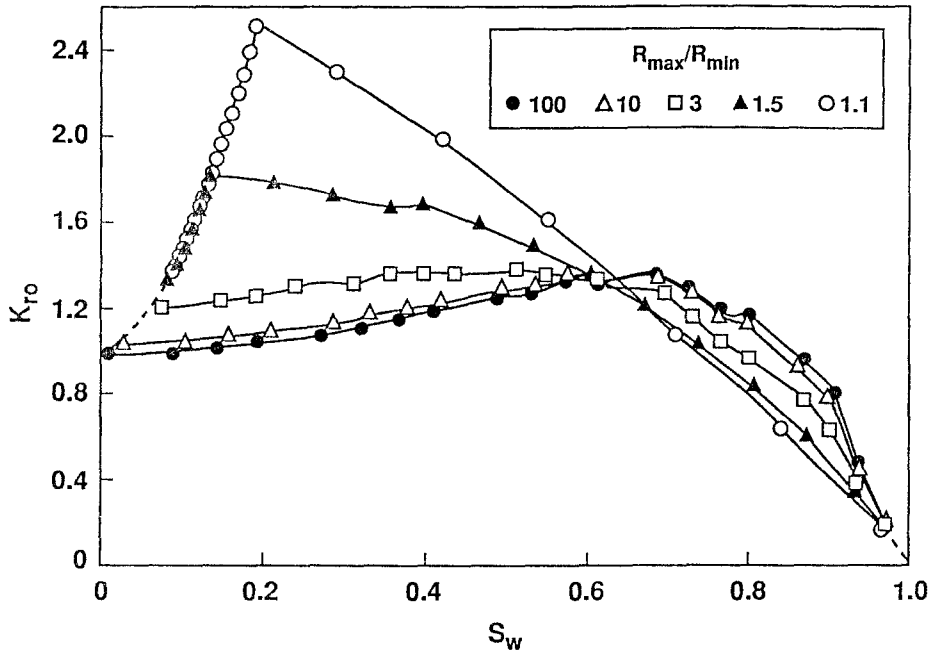

Fig. 7. K_{ro} vs R_{max}/R_{min} for a bundle of square tubes with $\mu_o/\mu_w = 30$.

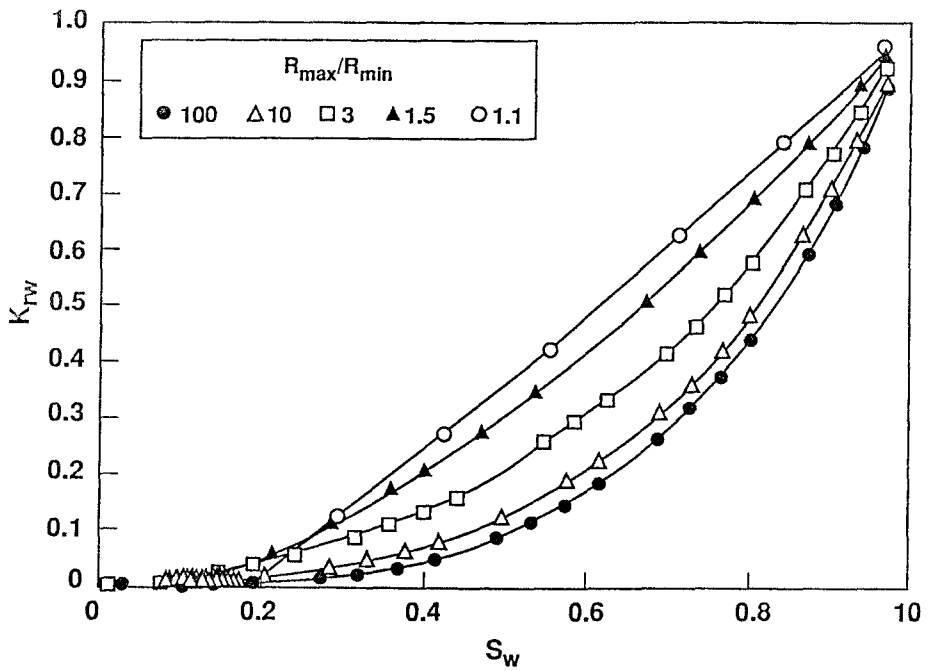

Fig. 8. K_{rw} vs R_{max}/R_{min} for a bundle of square tubes with $\mu_o/\mu_w = 30$.

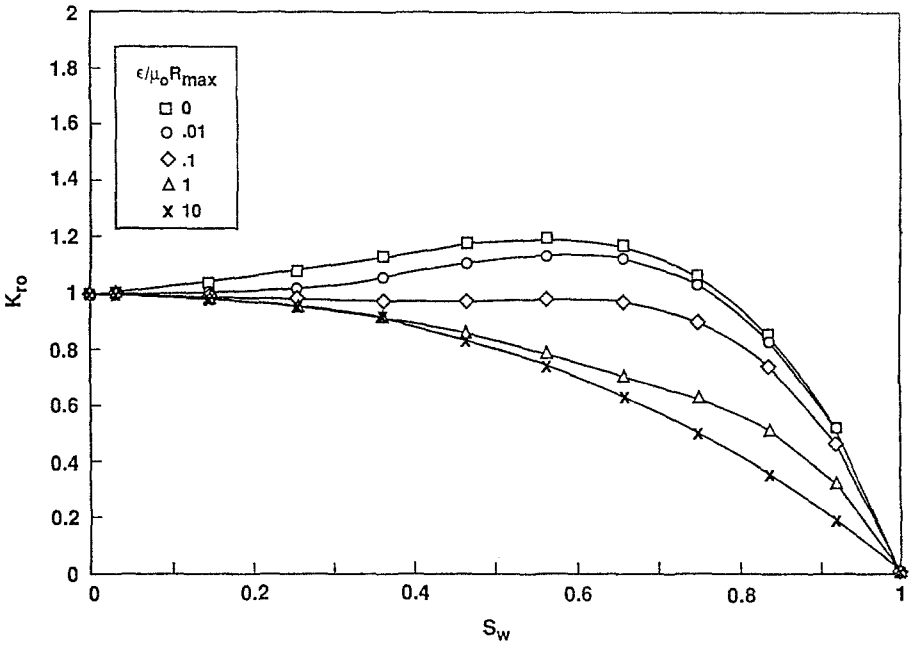

Fig. 9. Oil relative permeability vs dimensionless interfacial shear viscosity for a bundle of square tubes with $R_{max}/R_{min} = 10$ and $\mu_o/\mu_w = 10$.

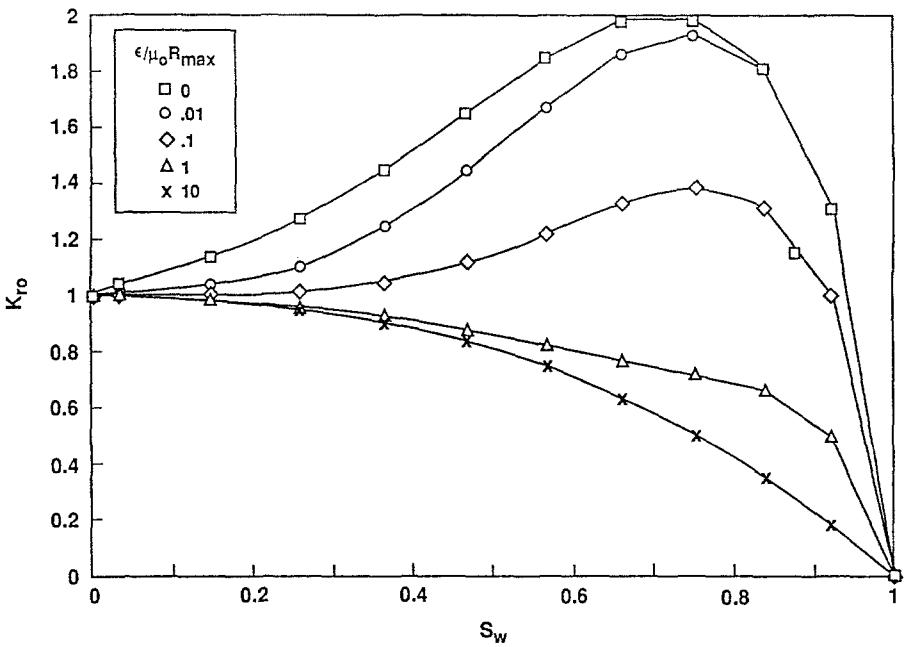

Fig. 10. Oil relative permeability vs. dimensionless interfacial shear viscosity for a bundle of square tubes with $R_{max}/R_{min} = 10$ and $\mu_o/\mu_w = 100$.

$\mu_o/\mu_w > 1$, oil relative permeability is greater than one over a significant range of S_w and increases with increasing μ_o/μ_w (Figure 2). Water relative permeability shows little sensitivity to μ_o/μ_w (Figure 3). As would be expected, the lubrication effect diminishs as the tube cross-section becomes more circular (as the number of sides increases in Figure 5). For a 16-side polygon cross section tube, viscosity ratio has much less of an effect on oil relative permeability (Figure 4). Again, water relative permeability is less sensitive to geometry (Figure 6). Including a distribution of pore sizes has an important effect in the predicted level of viscous coupling. Figure 7 shows that increasing the pore size range significantly reduces the level of viscous coupling as measured by the extent to which the maximum value of k_{ro} exceeds 1. Surprisingly, beyond about one order of magnitude, further increasing the pore size range has little effect and there is always some lubrication. These same types of results are obtained for other viscosity ratios greater than one and for other polygon shapes. The sharp change in slope in the k_{ro} curves as water saturation increases from zero for closely spaced distributions represents the point where the smallest tubes can no longer contain oil. As water saturation increases from that point, elimination of oil flow in smaller tubes is more important than increased lubrication in larger tubes and k_{ro} decreases.

The effect of nonzero interfacial shear viscosity is to reduce lubrication of oil by water (Figures 9 and 10). For $N_\varepsilon > 10$, there is no lubrication (oil-water interfaces act as no-slip boundaries) and oil relative permeability is independent of viscosity ratio. The k_{ro} curves for $N_\varepsilon = 10$ are identical to curves for zero interfacial shear viscosity and very low oil-water viscosity ratio (Figure 2). For $0 < N_\varepsilon < 10$, lubrication is important at high water saturations and reduced or eliminated at low water saturations. This results from the greater influence of interfacial shear viscosity at high interface curvatures associated with low water saturations.

For oil-water systems with no surface activity, surface viscous effects would not be expected (Stoodt and Slattery, 1984). Such systems should flow in porous media with $N_\varepsilon = 0$. Crude oils, however, do contain naturally occurring surface active compounds that accumulate at oil-water interfaces. Interfacial shear viscosity measurements for crude oil-brine systems were reported by Wasan and Mohan (1977). Their data is given in Table I. If a maximum pore radius of 0.01 cm is assumed, N_ε for these systems would range from 10 to 200.

Table I. Interfacial properties of crude-oils and 1% NaCl brine (Wasan and Mohan, 1977)

Crude oil	Crude oil viscosity (cp)	Interfacial tension (dynes/cm)	Interfacial shear viscosity (dyne-sec/cm)
South Texas	4.2	2.3	$4.2 \times 10-3$
Oklahoma	6.2	12.9	$1.6 \times 10-2$
Middle East	8.2	16.8	$7.2 \times 10-2$
Gach Saran	20.0	28.5	$4 \times 10-1$

On the basis of the calculations presented here, we conclude that a viscosity ratio effect on the relative permeability to oil at oil-water viscosity ratios greater than one cannot be ruled out. The effect is less, however, than indicated in earlier publications which consider flow only in single tubes. There appears to be much less of a viscosity ratio effect on relative permeability to water and on relative permeability to oil at viscosity ratios less than or equal to one. The influence of interfacial shear viscosity is to reduce or eliminate this viscosity ratio effect.

A number of uncertainties resulting from the asumptions made in these calculations should be pointed out. One obvious deficiency in this work is that we do not model axial variations in pore cross-sections (pore bodies and pore throats) nor do we model multiple pore interconnections. The effect of this on our conclusions is uncertain.

Another possible deficiency is that the Boussinesq Newtonian surface fluid model may be an over-simplification of more complex phenomena (Levich, 1962) and that measured surface viscosities may not quantitatively represent pore scale processes.

An additional uncertainty in comparing these analytical results to measurements obtained in real rocks is that the latter can contain delicate clay mineral structures that are sensitive to the movement of fluid-fluid interfaces and equilibrate in different ways to fluids of different ionic content. These changes can affect hydraulic conductivities to the extent that other effects are masked.

These results suggest a few definitive experiments to examine the effects of viscous coupling in the absence of other effects. First, a series of steady-state relative permeability measurements could be carried out in a stable porous medium (e.g., a clean sand pack) at a range of oil-water viscosity ratios greater than one. Such a system would need to be completely free of surface active contaminants. Alternatively, a nonaqueous fluid could be used as the wetting phase. If these results confirm a significant level of viscous coupling, then they could be extended to real petroleum reservoir fluid pairs, and finally, to a range of real reservoir rock.

5. Conclusions

Flow calculations in a model of a porous medium consisting of bundles of noncircular cross section tubes are used to investigate the influence of viscous coupling on two-phase water-oil relative permeabilities. Analysis of these calculations leads to the following.

(1) Where surface rheological effects can be neglected, viscous coupling is important. This leads to a dependence of oil relative permeability on oil-water viscosity ratio for viscosity ratios greater than one for a range of pore cross-section shapes and pore size distributions. The coupling effect is much less for oil relative permeability at oil-water viscosity ratios less than one and for water relative permeability at all viscosity ratios. Also, coupling is less in models with a wide distribution of pore sizes than where distribution is only over a narrow range.

(2) Interfacial shear viscosity acts to reduce viscous coupling and the effects of oil-water viscosity ratio on relative permeability. For values of interfacial shear viscosity reported in the literature for crude oil-water systems, viscous coupling is unimportant and there is no effect of oil-water viscosity ratio on relative permeability.

Appendix: Calculations for Flow in a Single Tube

(a) SINGLE-PHASE FLOW

The calculations in this paper consider straight, horizontal tubes whose cross-sections are regular s-sided polygons (equilateral triangle, square, etc. - Figure A1).

For slow axial flow of a fluid of viscosity, μ, resulting from a pressure gradient, Gp, assuming the cylindrical coordinate system in Figure A1, the axial velocity, $v(r, \theta)$, is given by

$$\frac{1}{r}\frac{\mathrm{d}}{\mathrm{d}r}\left[r\frac{\mathrm{d}v}{\mathrm{d}r}\right]+\frac{1}{r^2}\frac{\mathrm{d}^2v}{\mathrm{d}\Theta^2}=-\frac{Gp}{\mu} \tag{A1}$$

A general series solution, bounded at $r = 0$, for $v(r, \Theta)$ which considers symmetry of the geometry and flow with respect to the planes $\Theta = 0, \pm\pi/s, \pm 2\pi/s, \pm 3\pi/s$, etc. is

$$\frac{\mu v(r,\Theta)}{Gp}=-\frac{r^2}{4}+a_0+\sum_{n=1}^{n=\infty}[a_n r^{sn}\cos(sn\Theta)] \tag{A2}$$

subject to the boundary condition, $v(r, \Theta) = 0$ at the tube wall. To obtain successive approximations to $v(r, \Theta)$, we truncate the series at $n = N$. The positive definite integral over the tube wall

$$J[a_n]=\int_{S_t}[v^2(r,\Theta)]\,\mathrm{d}S_t \tag{A3}$$

is then minimized with respect to each of the undetermined parameter, $a_0, a_1, a_2, \ldots, a_N$. The set of $N + 1$ linear equations thus obtained is solved to obtain the parameters. The velocity profile is integrated over the tube cross section to obtain an expression for flow rate of the form

$$Q = -FR^4Gp/\mu \tag{A4}$$

The series for $v(r, \Theta)$ converges quickly. The $N \to \infty$ value for F is obtained to within 1 part in 10,000 with $N = 3$. For an equilateral triangle ($S = 3$), the exact solution $F = 1.35/\sqrt{3}$, (Singhal and Somerton, 1970) is obtained. For $S \to \infty$, the Poiseuille equation with $F = \pi/8$, is obtained.

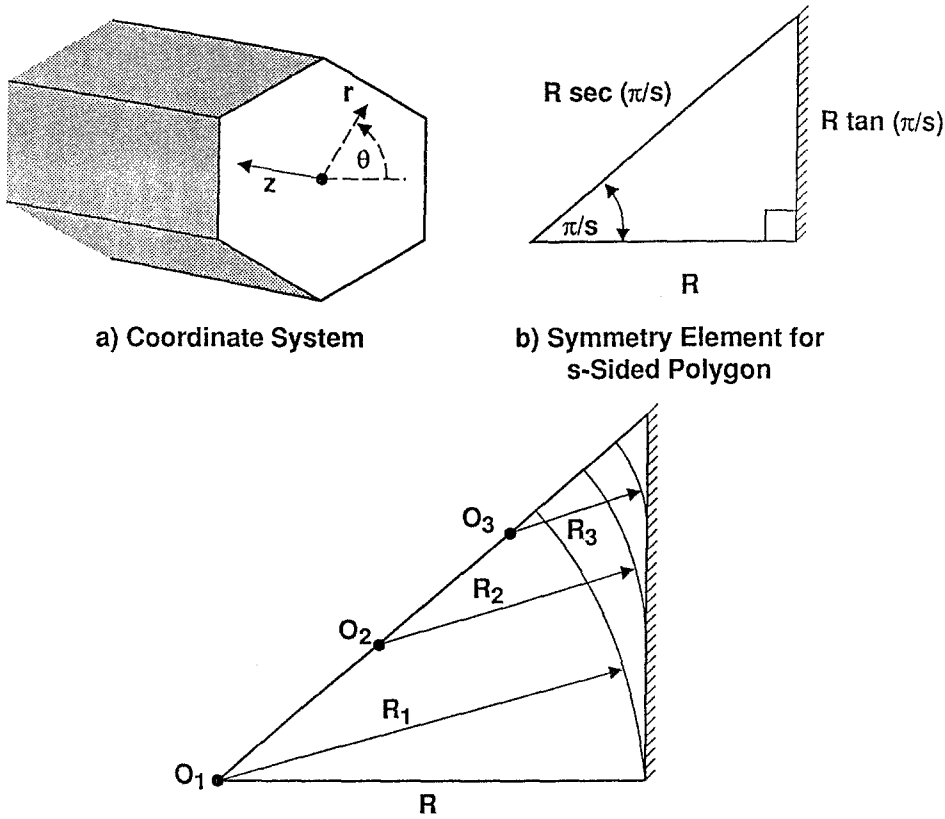

If aR = Distance From Center of Interface Circular Segment to Center of Polygon ($0 \leq a \leq \sec \pi/s$)

Then:

Interface Radius	$= R(1 - a \cos \pi/s)$
Water Saturation as a Fraction of Tube Volume	$= (1 - a \cos \pi/s)^2 [1 - \pi/(s \tan \pi/s)]$

Fig. A1. Polygon tube geometry.

(b) TWO-PHASE FLOW

For flow of two phases, oil and water, the velocity distributions, $v_o(r, \Theta)$ and $v_w(r, \Theta)$ are defined by (A1) in each phase subject to the zero velocity boundary condition at the tube wall and continuity of velocity and a stress balance across the oil-water interface.

With the assumption of low capillary number and negligible gravity, the normal stress balance at the oil-water interface in this geometry is satisfied only if interfaces

in the r–Θ plane are circular arcs. That is, interfacial tension locally dominates viscous gradient forces so that the interface must be a surface of constant curvature. Figure A1 shows the family of interface configurations that satisfy this requirement as well as the zero contact angle condition and gives the phase volume relationships for each. As discussed in the text, we assume that the minimum oil volume that can exist corresponds to a full circle internally tangent to the tube wall.

The tangential component of the stress balance (Aris, 1962) in the cylindrical coordinate system is

$$\mu_o\left[n_r\frac{\mathrm{d}v_o}{\mathrm{d}r}+\frac{n_\Theta}{r}\frac{\mathrm{d}v_o}{\mathrm{d}\Theta}\right]-\mu_w\left[n_r\frac{\mathrm{d}v_w}{\mathrm{d}r}+\frac{n_\Theta}{r}\frac{\mathrm{d}v_w}{\mathrm{d}\Theta}\right]-\frac{\varepsilon}{Row^2}\frac{\mathrm{d}^2v}{\mathrm{d}\Phi^2}=0, \tag{A5}$$

where ε is the Boussinesq surface shear viscosity and Row is the oil-water interface radius as shown in Figure A1. The variable Φ is the angular coordinate in a second cylindrical coordinate system whose origin is at the center of the interface circle (01, 02, 03 in Figure A1). Derivation of a general expression for $\mathrm{d}^2v/\mathrm{d}\Phi^2$ in terms of r and Θ derivatives by coordinate transformation is straightforward but results in an expression too complex to be given here.

For $\varepsilon = 0$, (A5) reduces to a statement of tangential stress continuity.

Solving (A1) in each phase subject to symmetry and boundedness requirements gives

$$\frac{\mu_o v_o(r,\Theta)}{Gp}=-\frac{r^2}{4}+a_0+\sum_{n=1}^{n=\infty}[a_n r^{sn}\cos(sn\Theta)], \tag{A6}$$

$$\frac{\mu_w v_w(r,\Theta)}{Gp}=-\frac{r^2}{4}+b_0+$$

$$+\sum_{n=1}^{n=\infty}[\{b_n r^{sn}+c_n r^{-sn}\}\cos(sn\Theta)]. \tag{A7}$$

Note that v_w is not required to be bounded at $r = 0$. A $\ln(r)$ term which appears in the general solution for v_w can be shown to vanish in satisfying the stress boundary condition (A5).

To satisfy the boundary conditions, three positive definite integrals are defined which will approach zero as the boundary conditions are satisfied. On the tube wall, S_t,

$$J_1[a_n,b_n,c_n]=\int_{S_t}[v(r,\Theta)]^2\,\mathrm{d}S_t, \tag{A8}$$

at the oil-water interface, S_i,

$$J_2[a_n,b_n,c_n]=\int_{S_i}[v_o(r,\Theta)-v_w(r,\Theta)]^2\,\mathrm{d}S_i, \tag{A9}$$

Table II. Two-phase flow calculation results for values of N square tubes, water saturation = 0.2146, $\varepsilon = 0$

Oil-water viscosity ratio = 0.1

N	F_o	F_w	J_1	J_2	J_3	$J_1 + J_2 + J_3$
1	0.4099	0.0389	5.6E-05	4.0E-08	2.9E-07	5.6E-05
2	0.4092	0.0353	2.2E-07	2.3E-10	4.2E-10	2.2E-07
3	0.4092	0.0354	2.6E-08	9.3E-12	7.6E-12	2.6E-08
4	0.4092	0.0354	2.5E-08	3.9E-11	2.5E-11	2.5E-08
5	0.4092	0.0354	8.8E-10	1.1E-12	5.0E-13	8.8E-10

Oil-water viscosity ratio = 1.0

N	F_o	F_w	J_1	J_2	J_3	$J_1 + J_2 + J_3$
1	0.5332	0.0303	4.3E-06	1.3E-07	8.3E-09	4.4E-06
2	0.5331	0.0293	1.4E-07	3.9E-09	7.9E-11	1.4E-07
3	0.5331	0.0292	1.3E-08	2.7E-10	3.1E-12	1.3E-08
4	0.5331	0.0292	2.2E-09	3.3E-11	2.4E-13	2.2E-09
5	0.5331	0.0292	5.1E-10	5.9E-12	3.0E-14	5.2E-10

Oil-water viscosity ratio = 10.

N	F_o	F_w	J_1	J_2	J_3	$J_1 + J_2 + J_3$
1	1.4073	0.0169	3.4E-05	6.7E-06	4.3E-09	4.1E-05
2	1.2700	0.0166	1.2E-05	3.4E-06	8.6E-10	1.5E-05
3	1.1859	0.0154	2.8E-06	9.9E-07	1.4E-10	3.8E-06
4	1.1554	0.0153	1.1E-06	4.1E-07	3.7E-11	1.5E-06
5	1.1390	0.0151	4.6E-07	1.8E-07	1.1E-11	6.4E-07
6	1.1310	0.0151	2.3E-07	8.7E-08	3.9E-12	3.2E-07
7	1.1262	0.0151	1.2E-07	4.4E-08	1.5E-12	1.6E-07
8	1.1235	0.0151	6.4E-08	2.4E-08	6.6E-13	8.8E-08
9	1.1218	0.0150	3.5E-08	1.3E-08	3.0E-13	4.8E-08
10	1.1208	0.0150	2.1E-08	7.9E-09	1.4E-13	2.9E-08

Oil-water viscosity ratio = 30.

N	F_o	F_w	J_1	J_2	J_3	$J_1 + J_2 + J_3$
1	3.2919	0.0148	4.7E-05	1.2E-05	8.2E-10	5.9E-05
2	2.6859	0.0137	1.8E-05	6.4E-06	1.9E-10	2.4E-05
3	2.2688	0.0116	5.5E-06	2.4E-06	4.2E-11	7.9E-06
4	2.0736	0.0111	2.7E-06	1.2E-06	1.4E-11	3.9E-06
5	1.9494	0.0107	1.4E-06	6.6E-07	5.4E-12	2.1E-06
6	1.8727	0.0105	8.1E-07	3.9E-07	2.4E-12	1.2E-06
7	1.8190	0.0102	4.9E-07	4.9E-07	1.1E-12	7.3E-07
8	1.7820	0.0101	3.2E-07	1.6E-07	6.0E-13	4.8E-07
9	1.7547	0.0100	2.1E-07	1.0E-07	3.3E-13	3.1E-07
10	1.7348	0.0100	1.5E-07	7.2E-08	1.9E-13	2.2E-07
11	1.7196	0.0099	1.0E-07	5.1E-08	1.1E-13	1.5E-07
12	1.7081	0.0099	7.3E-08	3.7E-08	6.8E-14	1.1E-07
13	1.6990	0.0098	5.3E-08	2.7E-08	4.3E-14	8.0E-08
14	1.6920	0.0098	4.0E-08	2.0E-08	2.8E-14	6.0E-08
15	1.6863	0.0098	3.0E-08	1.5E-08	1.9E-14	4.5E-08

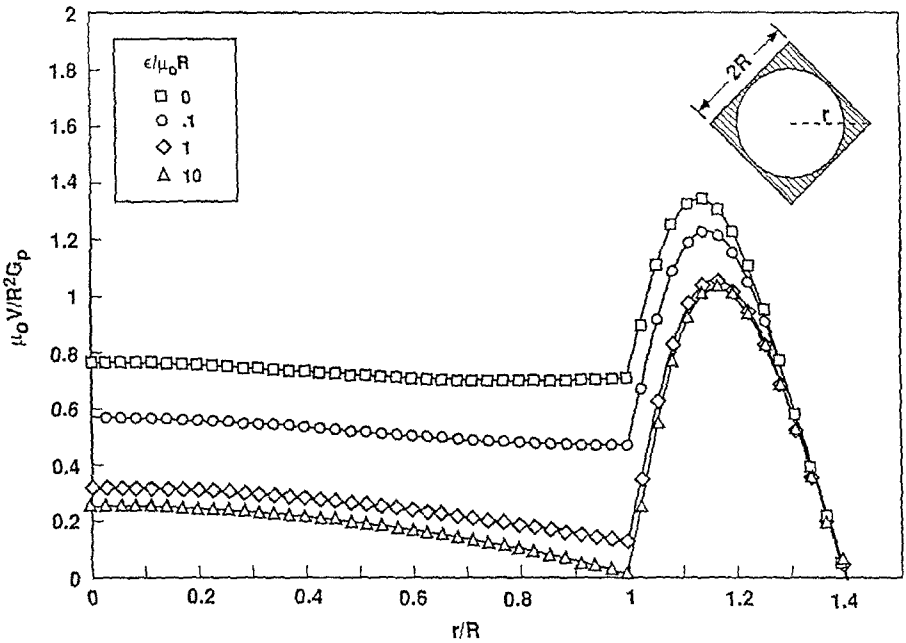

Fig. A2. Axial velocity profile along the diagonal of a square capillary tube as a function of dimensionless interfacial shear viscosity. Tube $S_w \approx 0.2146$. $\mu_o/\mu_w = 100$.

and

$$J_3[a_n, b_n, c_n] = \int_{S_i} [X(r, \Theta)]^2 \, dS_i. \tag{A10}$$

where $X(r, \Theta)$ is the left side of Equation (A5). To obtain successive approximations to $v_o(r, \Theta)$ and $v_w(r, \Theta)$, we truncate the series at $n = N$ and minimize the sum of the three integrals with respect to each of the undetermined parameters (the a's, b's and c's) and the set of $3N + 2$ linear equations solved to find a 'best' solution. Oil and water flow rates are calculated by integrating each velocity profile over its respective cross-section, giving the expressions

$$Q_o = -F_o R^4 Gp/\mu_o, \tag{A11}$$

$$Q_w = -F_w R^4 Gp/\mu_w. \tag{A12}$$

Table II. illustrates how the calculation progresses for two-phase flow in a square tube at a several oil-water viscosity ratios and with zero surface viscosity. Note that each of the three boundary integrals decreases with increasing N indicating progressively better approximations to the boundary conditions individually as well as in aggregate. As shown in Table II., convergence requires successively more parameters as the oil-water viscosity ratio increases.

As ε increases, velocity in the interface decreases. At very high values of ε, the interface behaves as a rigid boundary for flow of both oil and water. This can be seen

in Figure A2 which shows representative velocity profiles in a square tube as a function of $\varepsilon/\mu_o R$ with an oil-water viscosity ratio of 100. For high values of ε, our calculations agree with those of Ransohoff and Radke (1988), who considered corner flows in noncircular pores.

References

Aris, R., 1962, *Vectors, Tensors, and the Basic Equations of Fluid Mechanics*, Prentice-Hall, Englewood Cliffs, N.J.

Aziz, K. and Settari, A., 1979, *Petroleum Reservoir Simulation*, Applied Science Publishers, London.

Bear, J., 1972, *Dynamics of Fluids in Porous Media*, American Elsevier, New York.

Heiba, A. A., Davis, H. T., and Scriven, L. E., 1983, Effect of Wettability on two-phase relative permeabilities and capillary pressure, SPE 12172, SPE Fall Meeting, San Francisco.

Kalaydjian, F., 1990, Origin and quantification of coupling between relative permeabilities for two-phase flows in porous media, *Transport in Porous Media* **5**, 215–229.

Leverett, M. C., 1939, Flow of oil-water mixtures through unconsolidated sands, *Pet. Trans. AIME* **132**, 149–169.

Levich, V. G., 1962, *Physicochemical Hydrodynamics*, Prentice-Hall, Englewoood Cliffs, N.J.

Lin, C. Y. and Slattery, J. C., 1982, Three-dimensional, randomized, network model for two-phase flow through porous media, *AIChE J.* **28**, 2, 311–324.

Mason, G. and Morrow, N. R., 1987, Meniscus configurations and curvatures in non-axisymmetric pores of open and closed uniform cross section, *Proc. R. Soc. Lond. A* **414**, 111–133.

Odeh, A. S., 1959, Effect of viscosity ratio of relative permeability, *Pet. Trans. AIME* **216**, 346–353.

Peaceman, D. W., 1977, *Fundamentals of Numerical Reservoir Simulation*, Elsevier, New York.

Ransohoff, T. C. and Radke, C. J., 1988, *J. Colloid Interface Sci.* **121**(2), 392–401.

Rose, W., 1990, Coupling coefficients for two-phase flow in pore spaces of simple goemetry, *Transport in Porous Media* **5**, 97–102.

Scriven, L. E., 1960, Dynamics of a fluid interface, *Chem. Eng. Sci.* **12**, 98–108.

Singhal, A. K. and Somerton, W. H., 1970, Two-phase flow through a non-circular capillary at low reynodls number, *J. Can. Pet. Technol.* (July-Sept.), 197–205.

Slattery, J. C., 1972, *Momentum, Energy, and Mass Transfer in Continua*, McGraw-Hill, New York.

Stoodt, T. J. and Slattery, J. C., 1984, Effect of interfacial viscosities upon displacement, *AIChE J.* **30**(4), 564–568.

Wasan, D. T. and Mohan, V., 1977, Interfacial rheological properties of fluid interfaces containing surfactants, in D. O. Shah and R. S. Schechter, (eds), *Improved Oil Recovery by Surfactant and Polymer Flooding*, Academic Press, New York.

Whitaker, S., 1986a, Flow in porous media I: a theoretical derivation of Darcy's law, *Transport in Porous Media* **1**, 3–25.

Whitaker, S., 1986b, flow in porous media II: the governing equations of immiscible, two-phase flow, *Transport in Porous Media* **1**, 105–125.

Yuster, S. T., 1951, Theoretical considerations of multiphase flow in idealized capillary systems, *Proc. Third World Petroleum Congress, Section II*, 437–445.